Aqueous Self-Assembly of a Protein-Mimetic Ampholytic Block Copolypeptide

Jing Sun,[†§] *Peter Černoch,*[‡§] *Antje Völkel,*[§] *Yuhan Wei,*[†] *Janne Ruokolainen,*[∥] *and Helmut Schlaad*[⊥§]

[†] School of Polymer Science and Engineering, Qingdao University of Science and Technology, 53 Zhengzhou Road, Qingdao 266042, China. [‡] Institute of Macromolecular Chemistry, Heyrovského nám. 2, 162 06 Praha 6, Czech Republic. [§] Department of Colloid Chemistry, Max Planck Institute of Colloids and Interfaces, Research Campus Golm, 14424 Potsdam, Germany. [∥] Department of Applied Physics, Aalto University Nanomicroscopy Center (Aalto-NMC), Puumiehenkuja 2, 02150 Espoo, Finland, [⊥] University of Potsdam, Institute of Chemistry, Karl-Liebknecht-Str. 24-25, 14476 Potsdam, Germany.

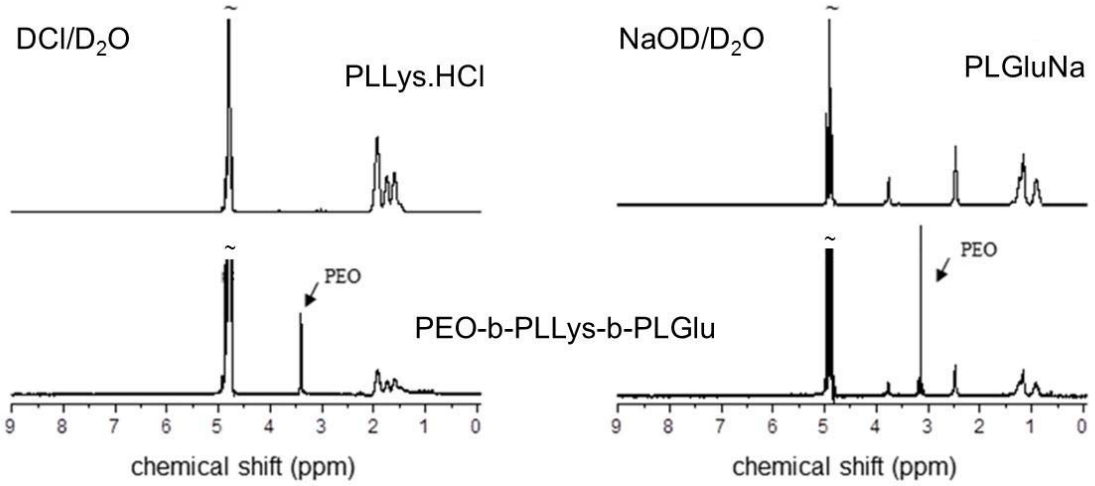

Figure S1. ^{1}H NMR spectra (400.1 MHz, r.t.) of PLLys and PEO_{42}-*b*-$PLLys_{61}$-*b*-$PLGlu_{62}$ in 0.9 M DCl in D_2O (left) and PLGlu and PEO_{42}-*b*-$PLLys_{61}$-*b*-$PLGlu_{62}$ in 1.0 M NaOD in D_2O (right).

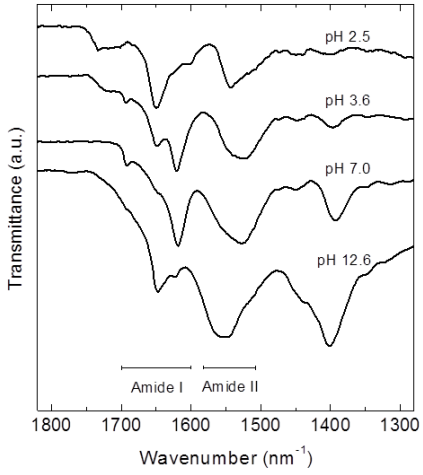

Figure S2. FT-IR spectra of freeze-dried samples of 0.2 wt% PEO_{42}-$PLLys_{61}$-$PLGlu_{62}$ in water at pH 2.5–12.6.

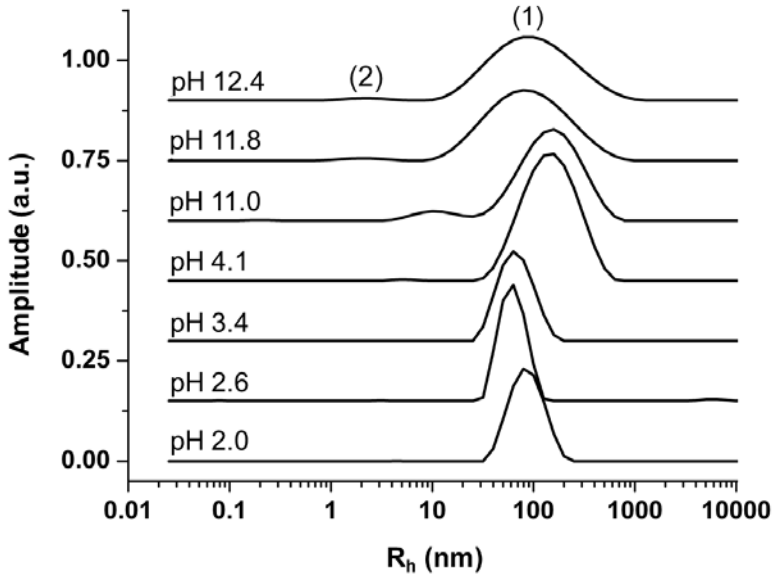

Figure S3. Normalized distributions of hydrodynamic radii (R_h) observed in ~0.1 wt% solutions of PEO_{42}-*b*-$PLLys_{61}$-*b*-$PLGlu_{62}$ in 0.5 M NaCl at various pH. Data measured at scattering angle 90° at room temperature. (1) and (2) denote slow and fast modes, respectively.

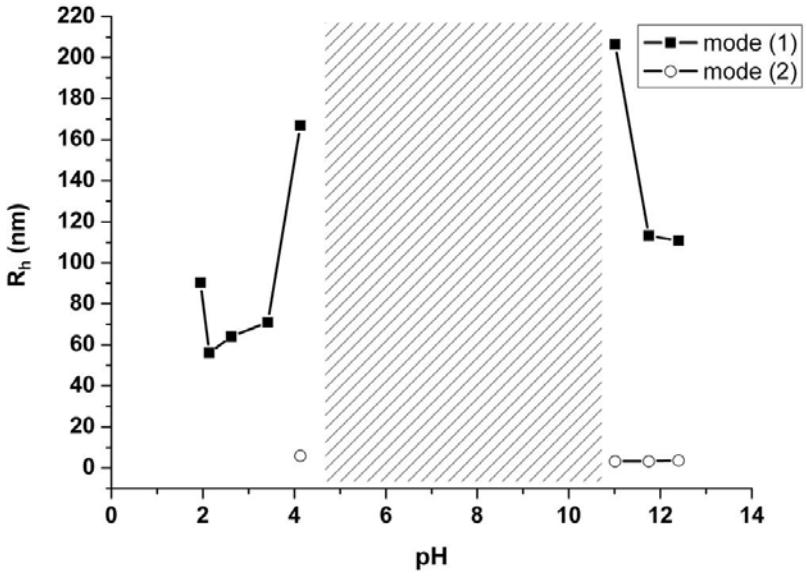

Figure S4. Dependence of hydrodynamic radii (R_h) observed in ~0.1 wt% solutions of PEO_{42}-*b*-$PLLys_{61}$-*b*-$PLGlu_{62}$ in 0.5 M NaCl at various solution pH. Data measured at scattering angle 90° at room temperature. The hatched area represents an unstable region where all solutions demonstrate tendency to precipitate. Mode (1) is related to the major, slow diffusive mode of large aggregates, while mode (2) identifies the fast dynamic process of coupled diffusion of polyions and counterions or single chains.

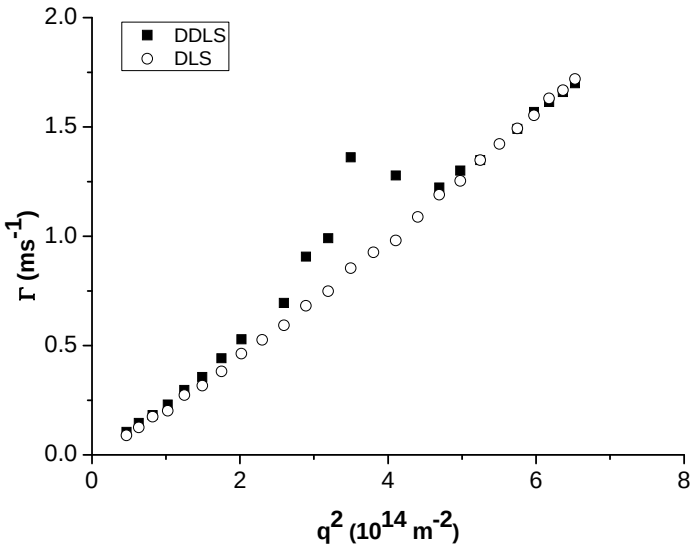

Figure S5. Relaxation rates (Γ) obtained by DLS and DDLS as a function of the square of the scattering vector (q^2) for the ~0.1 wt% solutions of PEO_{42}-$PLLys_{61}$-$PLGlu_{62}$ in 0.5 M aqueous NaCl at pH 2.0.

DLS and DDLS gives linear dependence of decay rate with square of the scattering vector passing the origin [0,0]. The observable deviation around scattering angle of ~90° might be caused by either simultaneous presence of two diffusional effects with similar correlation times, which cannot be distinguished by the fitting algorithm, or deviation of the shape of the scattered objects from an ideal sphere. However, as there is not shift in the Γ-axis, which would indicate a contribution of rotational diffusion (Lehner et al. *Langmuir* **2000**, *16*, 1689-1695), the scattered objects are considered to be spherical in shape.

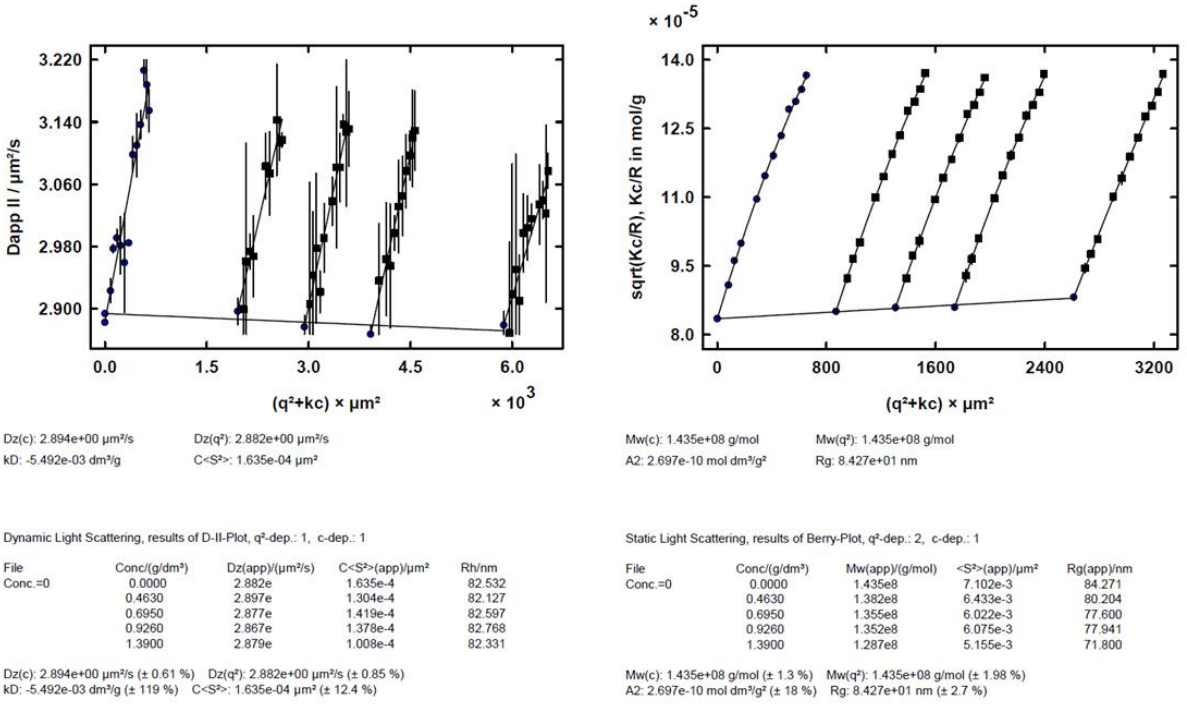

Dynamic Light Scattering, results of D-II-Plot, q²-dep.: 1, c-dep.: 1

File	Conc/(g/dm³)	Dz(app)/(µm²/s)	C<S²>(app)/µm²	Rh/nm
Conc.=0	0.0000	2.882e	1.635e-4	82.532
	0.4630	2.897e	1.304e-4	82.127
	0.6950	2.877e	1.419e-4	82.597
	0.9260	2.867e	1.378e-4	82.768
	1.3900	2.879e	1.008e-4	82.331

Dz(c): 2.894e+00 µm²/s (± 0.61 %) Dz(q²): 2.882e+00 µm²/s (± 0.85 %)
kD: -5.492e-03 dm³/g (± 119 %) C<S²>: 1.635e-04 µm² (± 12.4 %)

Static Light Scattering, results of Berry-Plot, q²-dep.: 2, c-dep.: 1

File	Conc/(g/dm³)	Mw(app)/(g/mol)	<S²>(app)/µm²	Rg(app)/nm
Conc.=0	0.0000	1.435e8	7.102e-3	84.271
	0.4630	1.382e8	6.433e-3	80.204
	0.6950	1.355e8	6.022e-3	77.600
	0.9260	1.352e8	6.075e-3	77.941
	1.3900	1.287e8	5.155e-3	71.800

Mw(c): 1.435e+08 g/mol (± 1.3 %) Mw(q²): 1.435e+08 g/mol (± 1.98 %)
A2: 2.697e-10 mol dm³/g² (± 18 %) Rg: 8.427e+01 nm (± 2.7 %)

Figure S6. Concentration- and angle-dependent DLS (left) and SLS (right) data for 0.05–0.14 wt% PEO_{42}-$PLLys_{61}$-$PLGlu_{62}$ in 0.5 M aqueous NaCl at pH 2.0 at room temperature.

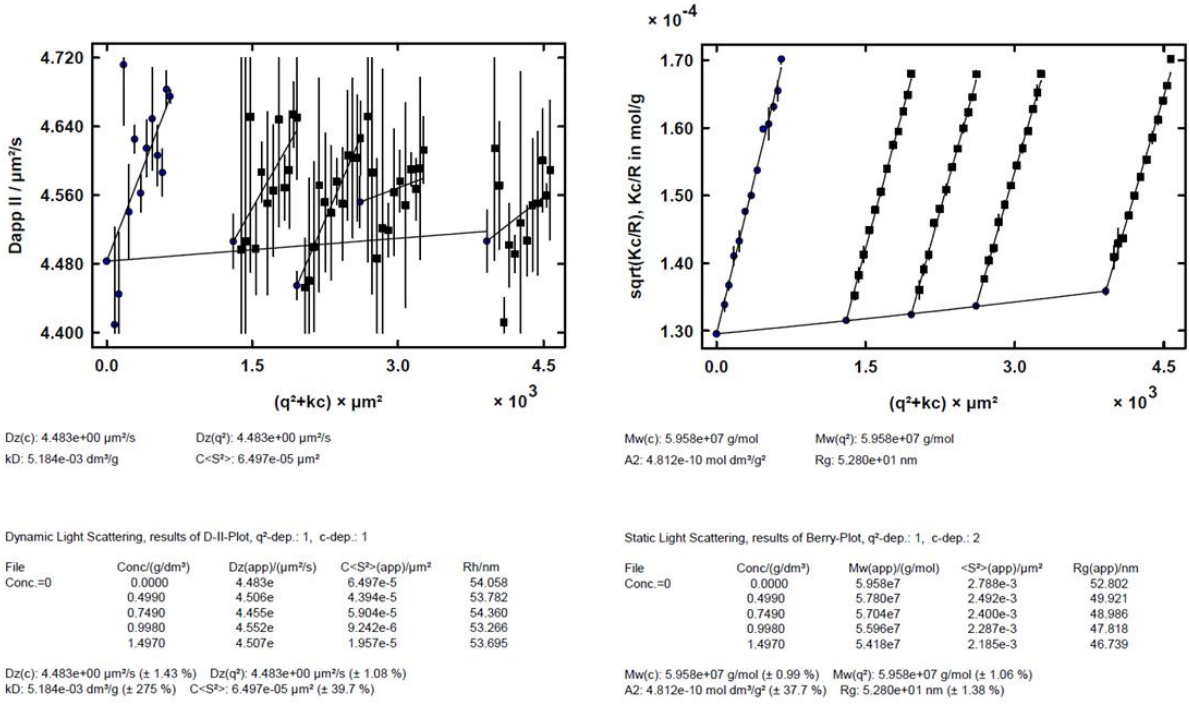

Dynamic Light Scattering, results of D-II-Plot, q²-dep.: 1, c-dep.: 1

File	Conc/(g/dm³)	Dz(app)/(µm²/s)	C<S²>(app)/µm²	Rh/nm
Conc.=0	0.0000	4.483e	6.497e-5	54.058
	0.4990	4.506e	4.394e-5	53.782
	0.7490	4.455e	5.904e-5	54.360
	0.9980	4.552e	9.242e-6	53.266
	1.4970	4.507e	1.957e-5	53.695

Dz(c): 4.483e+00 µm²/s (± 1.43 %) Dz(q²): 4.483e+00 µm²/s (± 1.08 %)
kD: 5.184e-03 dm³/g (± 275 %) C<S²>: 6.497e-05 µm² (± 39.7 %)

Static Light Scattering, results of Berry-Plot, q²-dep.: 1, c-dep.: 2

File	Conc/(g/dm³)	Mw(app)/(g/mol)	<S²>(app)/µm²	Rg(app)/nm
Conc.=0	0.0000	5.958e7	2.788e-3	52.802
	0.4990	5.780e7	2.492e-3	49.921
	0.7490	5.704e7	2.400e-3	48.986
	0.9980	5.596e7	2.287e-3	47.818
	1.4970	5.418e7	2.185e-3	46.739

Mw(c): 5.958e+07 g/mol (± 0.99 %) Mw(q²): 5.958e+07 g/mol (± 1.06 %)
A2: 4.812e-10 mol dm³/g² (± 37.7 %) Rg: 5.280e+01 nm (± 1.38 %)

Figure S7. Concentration- and angle-dependent DLS (left) and SLS (right) data for 0.05–0.15 wt% PEO_{42}-$PLLys_{61}$-$PLGlu_{62}$ in 0.5 M aqueous NaCl at pH 2.2 at room temperature.

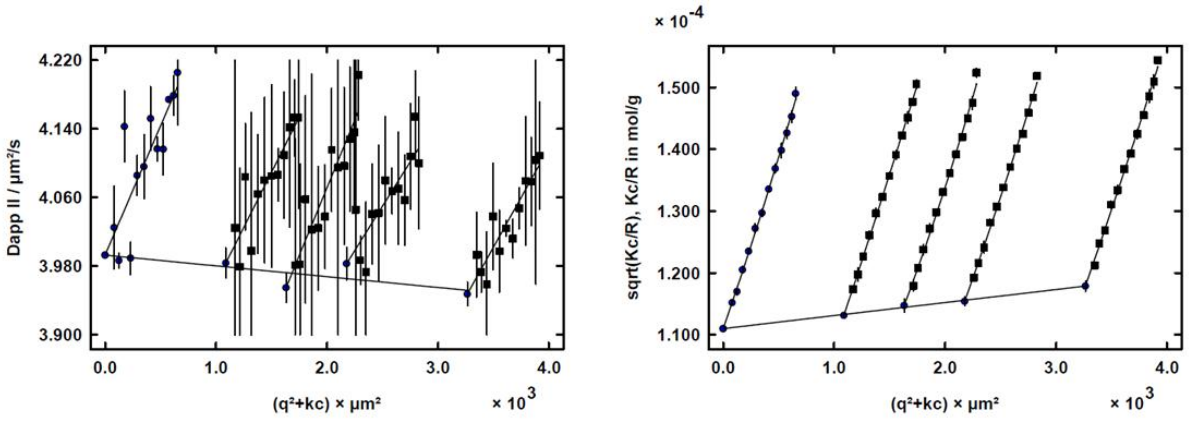

Dz(c): 3.993e+00 µm²/s Dz(q²): 3.993e+00 µm²/s
kD: -7.219e-03 dm³/g C<S²>: 7.540e-05 µm²

Mw(c): 8.118e+07 g/mol Mw(q²): 8.118e+07 g/mol
A2: 5.360e-10 mol dm³/g² Rg: 5.273e+01 nm

Dynamic Light Scattering, results of D-II-Plot, q²-dep.: 1, c-dep.: 1

File	Conc/(g/dm³)	Dz(app)/(µm²/s)	C<S²>(app)/µm²	Rh/nm
Conc.=0	0.0000	3.993e	7.540e-5	60.698
	0.4750	3.984e	6.447e-5	60.840
	0.7120	3.955e	7.984e-5	61.222
	0.9500	3.983e	5.197e-5	60.748
	1.4250	3.947e	5.881e-5	61.266

Dz(c): 3.993e+00 µm²/s (± 0.61 %) Dz(q²): 3.993e+00 µm²/s (± 0.72 %)
kD: -7.219e-03 dm³/g (± 88.7 %) C<S²>: 7.540e-05 µm² (± 22.7 %)

Static Light Scattering, results of Berry-Plot, q²-dep.: 2, c-dep.: 1

File	Conc/(g/dm³)	Mw(app)/(g/mol)	<S²>(app)/µm²	Rg(app)/nm
Conc.=0	0.0000	8.118e7	2.780e-3	52.727
	0.4750	7.813e7	2.855e-3	53.436
	0.7120	7.596e7	2.491e-3	49.911
	0.9500	7.508e7	2.605e-3	51.039
	1.4250	7.197e7	2.622e-3	51.201

Mw(c): 8.118e+07 g/mol (± 0.67 %) Mw(q²): 8.118e+07 g/mol (± 1.2 %)
A2: 5.360e-10 mol dm³/g² (± 8.05 %) Rg: 5.273e+01 nm (± 4.1 %)

Figure S8. Concentration- and angle-dependent DLS (left) and SLS (right) data for 0.05–0.14 wt% PEO_{42}-$PLLys_{61}$-$PLGlu_{62}$ in 0.5 M aqueous NaCl at pH 2.6 at room temperature.

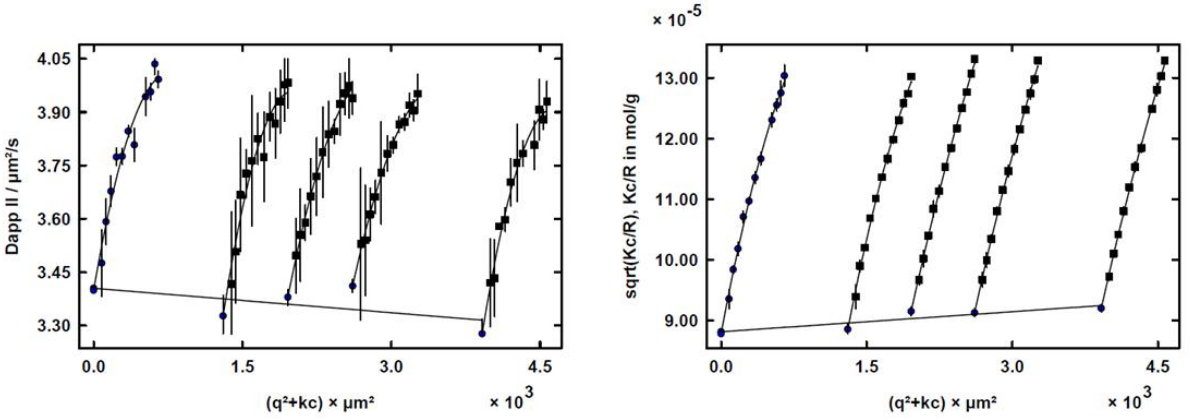

Dz(c): 3.405e+00 µm²/s Dz(q²): 3.400e+00 µm²/s
kD: -2.164e-02 dm³/g C<S²>: 4.747e-04 µm²

Mw(c): 1.286e+08 g/mol Mw(q²): 1.296e+08 g/mol
A2: 3.122e-10 mol dm³/g² Rg: 7.630e+01 nm

Dynamic Light Scattering, results of D-II-Plot, q²-dep.: 2, c-dep.: 1

File	Conc/(g/dm³)	Dz(app)/(µm²/s)	C<S²>(app)/µm²	Rh/nm
Conc.=0	0.0000	3.400e	4.747e-4	71.354
	0.4060	3.327e	5.433e-4	72.905
	0.6090	3.380e	4.222e-4	71.767
	0.8120	3.411e	3.769e-4	71.090
	1.2180	3.277e	5.288e-4	73.984

Dz(c): 3.405e+00 µm²/s (± 2.61 %) Dz(q²): 3.400e+00 µm²/s (± 1.58 %)
kD: -2.164e-02 dm³/g (± 147 %) C<S²>: 4.747e-04 µm² (± 21.5 %)

Static Light Scattering, results of Berry-Plot, q²-dep.: 2, c-dep.: 1

File	Conc/(g/dm³)	Mw(app)/(g/mol)	<S²>(app)/µm²	Rg(app)/nm
Conc.=0	0.0000	1.296e8	5.822e-3	76.299
	0.4060	1.274e8	5.555e-3	74.530
	0.6090	1.194e8	4.753e-3	68.941
	0.8120	1.199e8	4.764e-3	69.025
	1.2180	1.180e8	4.669e-3	68.328

Mw(c): 1.286e+08 g/mol (± 3.66 %) Mw(q²): 1.296e+08 g/mol (± 2.22 %)
A2: 3.122e-10 mol dm³/g² (± 55.2 %) Rg: 7.630e+01 nm (± 3.7 %)

Figure S9. Concentration- and angle-dependent DLS (left) and SLS (right) data for 0.04–0.12 wt% PEO_{42}-$PLLys_{61}$-$PLGlu_{62}$ in 0.5 M aqueous NaCl at pH 3.4 at room temperature.

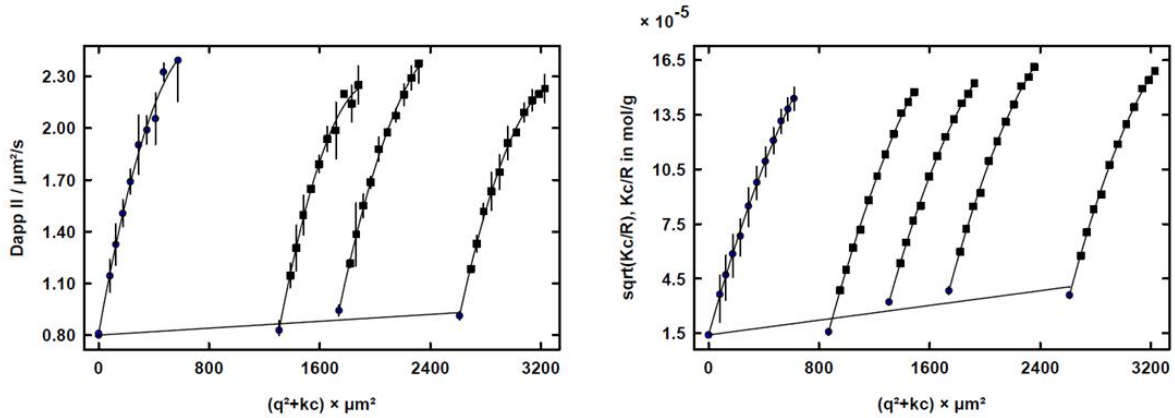

Dz(c): 8.001e-01 µm²/s Dz(q²): 8.104e-01 µm²/s
kD: 1.261e-01 dm³/g C<S²>: 5.525e-03 µm²

Mw(c): 5.046e+09 g/mol Mw(q²): 5.046e+09 g/mol
A2: 2.860e-10 mol dm³/g² Rg: 3.403e+02 nm

Dynamic Light Scattering, results of D-II-Plot, q²-dep.: 2, c-dep.: 1

File	Conc/(g/dm³)	Dz(app)/(µm²/s)	C<S²>(app)/µm²	Rh/nm
Conc.=0	0.0000	8.100e-1	5.525e-3	295.929
	0.6500	8.280e-1	5.133e-3	289.121
	0.8660	9.430e-1	3.997e-3	253.601
	1.3000	9.130e-1	4.049e-3	261.759

Dz(c): 8.001e-01 µm²/s (± 18.1 %) Dz(q²): 8.104e-01 µm²/s (± 8.78 %)
kD: 1.261e-01 dm³/g (± 148 %) C<S²>: 5.525e-03 µm² (± 14.3 %)

Static Light Scattering, results of Berry-Plot, q²-dep.: 2, c-dep.: 1

File	Conc/(g/dm³)	Mw(app)/(g/mol)	<S²>(app)/µm²	Rg(app)/nm
Conc.=0	0.0000	5.046e9	1.158e-1	340.252
	0.4330	3.970e9	1.058e-1	325.263
	0.6500	9.672e8	5.075e-2	225.270
	0.8660	6.790e8	4.370e-2	209.043
	1.3000	7.747e8	4.759e-2	218.155

Mw(c): 5.046e+09 g/mol (± 226 %) Mw(q²): 5.046e+09 g/mol (± 25.9 %)
A2: 2.860e-10 mol dm³/g² (± 130 %) Rg: 3.403e+02 nm (± 6.81 %)

Figure S10. Concentration- and angle-dependent DLS (left) and SLS (right) data for 0.04–0.13 wt% PEO_{42}-P$LLys_{61}$-P$LGlu_{62}$ in 0.5 M aqueous NaCl at pH 4.1 at room temperature.

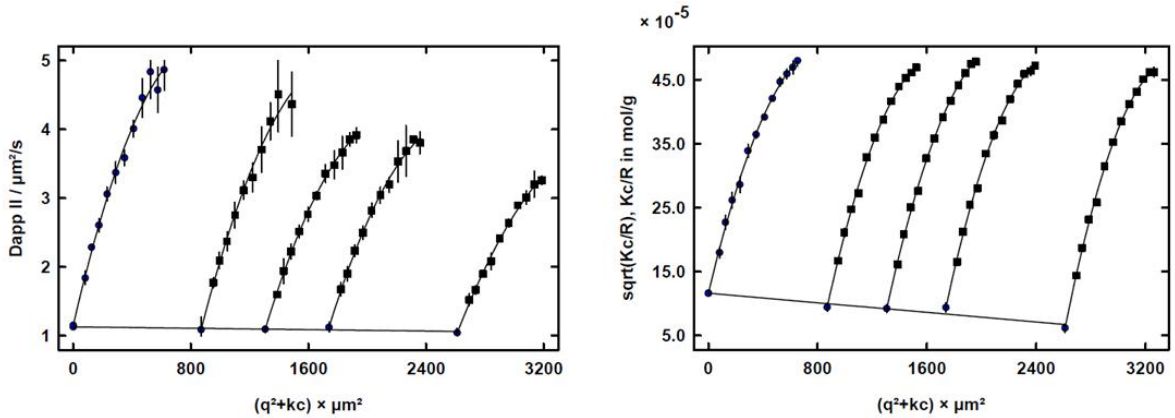

Dz(c): 6.284e-01 µm²/s Dz(q²): 6.510e-01 µm²/s
kD: -9.337e-02 dm³/g C<S²>: 1.420e-02 µm²

Mw(c): 7.419e+07 g/mol Mw(q²): 7.419e+07 g/mol
A2: -4.976e-09 mol dm³/g² Rg: 2.152e+02 nm

Dynamic Light Scattering, results of D-II-Plot, q²-dep.: 2, c-dep.: 1

File	Conc/(g/dm³)	Dz(app)/(µm²/s)	C<S²>(app)/µm²	Rh/nm
Conc.=0	0.0000	6.510e-1	1.420e-2	368.182
	0.3810	5.870e-1	1.416e-2	408.062
	0.5720	5.940e-1	1.181e-2	403.916
	0.7620	6.220e-1	1.112e-2	385.438
	1.1440	5.420e-1	1.008e-2	442.232

Dz(c): 6.284e-01 µm²/s (± 7.19 %) Dz(q²): 6.510e-01 µm²/s (± 27 %)
kD: -9.337e-02 dm³/g (± 100 %) C<S²>: 1.420e-02 µm² (± 29.8 %)

Static Light Scattering, results of Berry-Plot, q²-dep.: 2, c-dep.: 1

File	Conc/(g/dm³)	Mw(app)/(g/mol)	<S²>(app)/µm²	Rg(app)/nm
Conc.=0	0.0000	7.419e7	4.632e-2	215.219
	0.3810	1.129e8	6.153e-2	248.059
	0.5720	1.176e8	6.253e-2	250.051
	0.7620	1.138e8	6.339e-2	251.774
	1.1440	2.622e8	1.033e-1	321.464

Mw(c): 7.419e+07 g/mol (± 22.6 %) Mw(q²): 7.419e+07 g/mol (± 12 %)
A2: -4.976e-09 mol dm³/g² (± 39.4 %) Rg: 2.152e+02 nm (± 3.85 %)

Figure S11. Concentration- and angle-dependent DLS (left) and SLS (right) data for 0.04–0.11 wt% PEO_{42}-P$LLys_{61}$-P$LGlu_{62}$ in 0.5 M aqueous NaCl at pH 11.0 at room temperature.

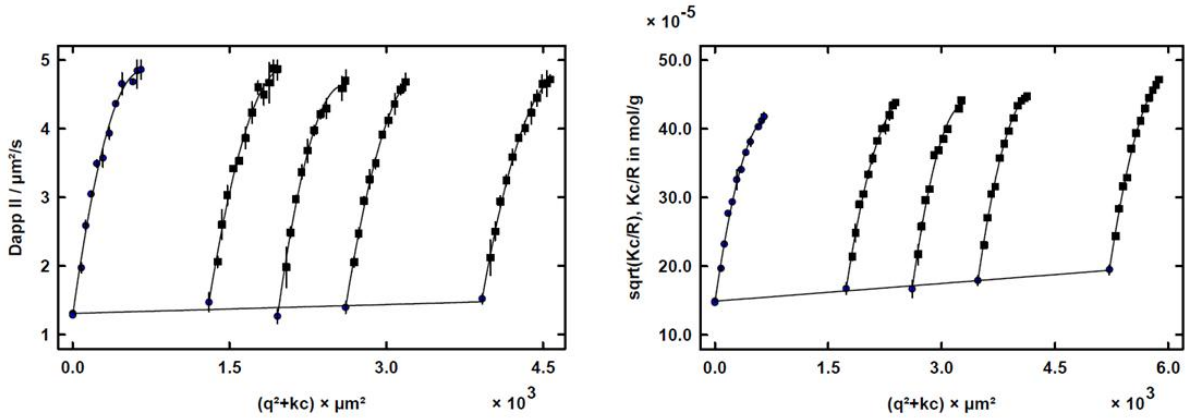

Dz(c): 1.308e+00 µm²/s Dz(q²): 1.285e+00 µm²/s
kD: 1.131e-01 dm³/g C<S²>: 8.446e-03 µm²

Mw(c): 4.505e+07 g/mol Mw(q²): 4.626e+07 g/mol
A2: 5.869e-09 mol dm³/g² Rg: 1.758e+02 nm

Dynamic Light Scattering, results of D-II-Plot, q²-dep.: 2, c-dep.: 1

File	Conc/(g/dm³)	Dz(app)/(µm²/s)	C<S²>(app)/µm²	Rh/nm
Conc.=0	0.0000	1.285e	8.446e-3	186.634
	0.3800	1.472e	6.370e-3	162.927
	0.5710	1.267e	8.499e-3	189.259
	0.7610	1.396e	6.743e-3	171.755
	1.1420	1.522e	5.689e-3	157.524

Dz(c): 1.308e+00 µm²/s (± 12.8 %) Dz(q²): 1.285e+00 µm²/s (± 12 %)
kD: 1.131e-01 dm³/g (± 148 %) C<S²>: 8.446e-03 µm² (± 15 %)

Static Light Scattering, results of Berry-Plot, q²-dep.: 2, c-dep.: 1

File	Conc/(g/dm³)	Mw(app)/(g/mol)	<S²>(app)/µm²	Rg(app)/nm
Conc.=0	0.0000	4.626e7	3.089e-2	175.764
	0.3800	3.573e7	2.534e-2	159.185
	0.5710	3.592e7	2.818e-2	167.880
	0.7610	3.113e7	2.528e-2	158.999
	1.1420	2.630e7	2.237e-2	149.567

Mw(c): 4.505e+07 g/mol (± 7.65 %) Mw(q²): 4.626e+07 g/mol (± 11.6 %)
A2: 5.869e-09 mol dm³/g² (± 18.9 %) Rg: 1.758e+02 nm (± 4.52 %)

Figure S12. Concentration- and angle-dependent DLS (left) and SLS (right) data for 0.04–0.11 wt% PEO_{42}-$PLLys_{61}$-$PLGlu_{62}$ in 0.5 M aqueous NaCl at pH 11.8 at room temperature.

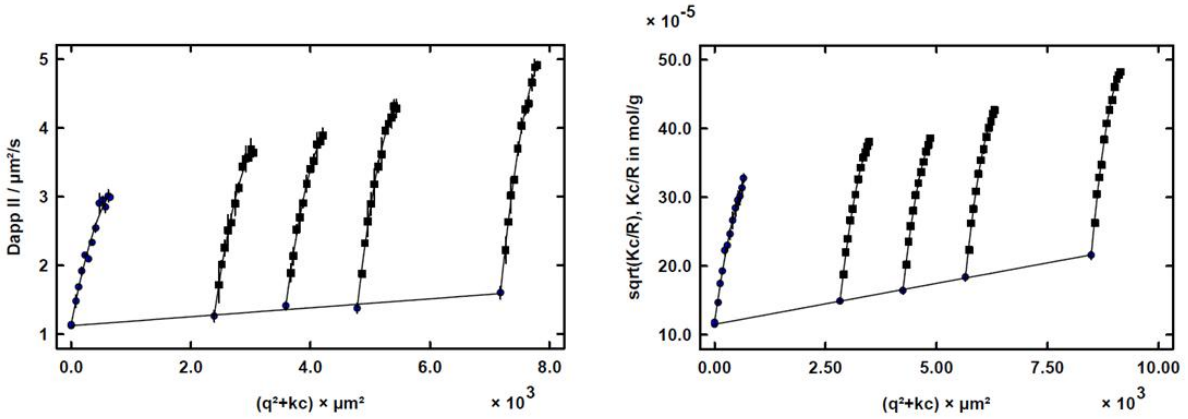

Dz(c): 1.123e+00 µm²/s Dz(q²): 1.138e+00 µm²/s
kD: 3.462e-01 dm³/g C<S²>: 4.055e-03 µm²

Mw(c): 7.553e+07 g/mol Mw(q²): 7.169e+07 g/mol
A2: 9.672e-09 mol dm³/g² Rg: 1.525e+02 nm

Dynamic Light Scattering, results of D-II-Plot, q²-dep.: 2, c-dep.: 1

File	Conc/(g/dm³)	Dz(app)/(µm²/s)	C<S²>(app)/µm²	Rh/nm
Conc.=0	0.0000	1.138e	4.055e-3	210.614
	0.4010	1.264e	4.847e-3	189.674
	0.6020	1.415e	4.579e-3	169.430
	0.8020	1.377e	5.571e-3	174.102
	1.2040	1.605e	5.382e-3	149.290

Dz(c): 1.123e+00 µm²/s (± 7.22 %) Dz(q²): 1.138e+00 µm²/s (± 11.2 %)
kD: 3.462e-01 dm³/g (± 26.8 %) C<S²>: 4.055e-03 µm² (± 20.7 %)

Static Light Scattering, results of Berry-Plot, q²-dep.: 2, c-dep.: 1

File	Conc/(g/dm³)	Mw(app)/(g/mol)	<S²>(app)/µm²	Rg(app)/nm
Conc.=0	0.0000	7.169e7	2.325e-2	152.464
	0.4010	4.504e7	2.289e-2	151.279
	0.6020	3.698e7	2.100e-2	144.899
	0.8020	2.958e7	2.030e-2	142.463
	1.2040	2.146e7	1.949e-2	139.610

Mw(c): 7.553e+07 g/mol (± 3.21 %) Mw(q²): 7.169e+07 g/mol (± 11.7 %)
A2: 9.672e-09 mol dm³/g² (± 3.13 %) Rg: 1.525e+02 nm (± 5.5 %)

Figure S13. Concentration- and angle-dependent DLS (left) and SLS (right) data for 0.04–0.12 wt% PEO_{42}-$PLLys_{61}$-$PLGlu_{62}$ in 0.5 M aqueous NaCl at pH 12.4 at room temperature.

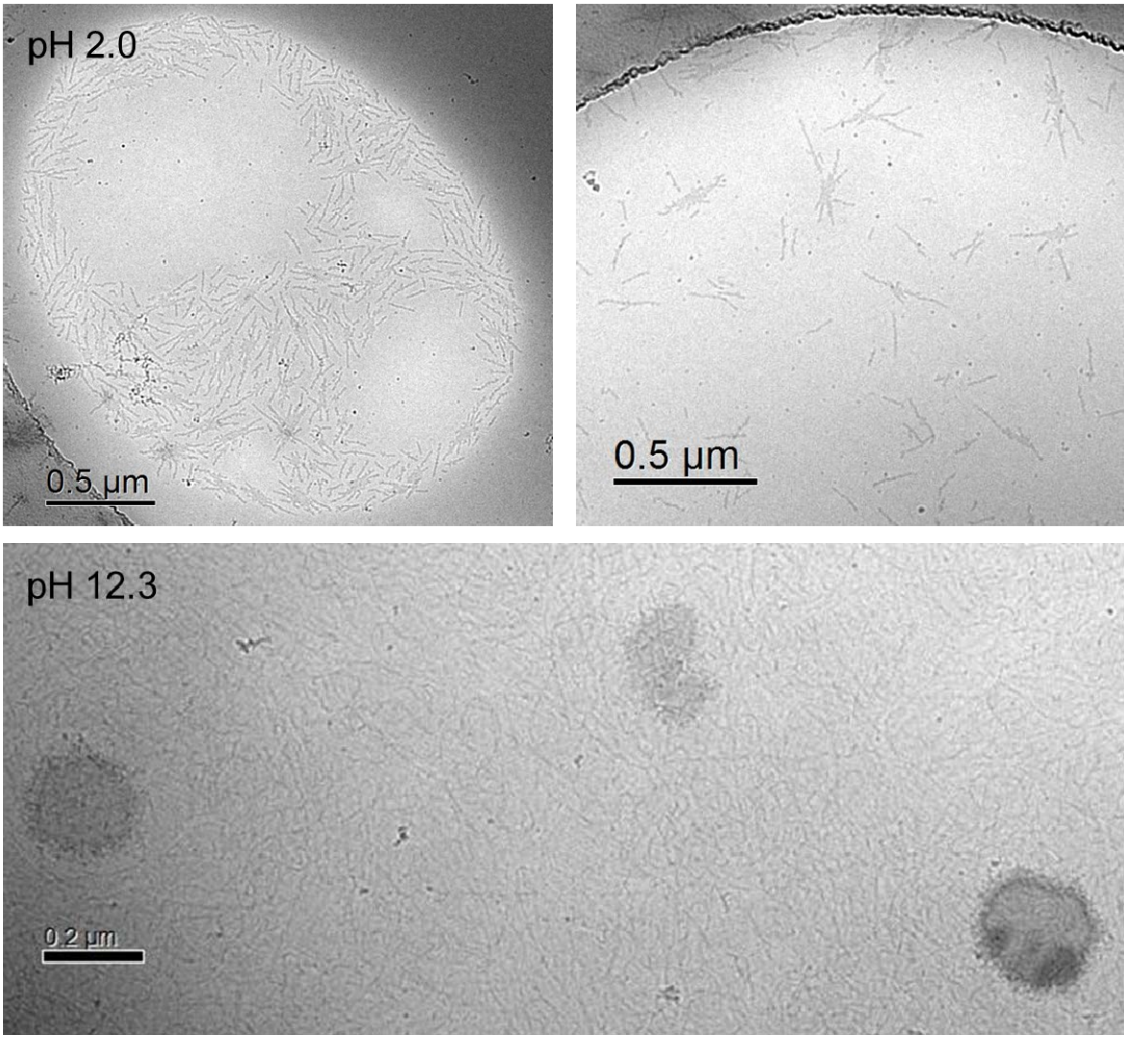

Figure S14. Exemplary cryogenic transmission electron micrographs of aged ~0.1 wt% solutions of PEO_{42}-*b*-$PLLys_{61}$-*b*-$PLGlu_{62}$ in 0.5 M NaCl at pH 2.0 (top) and pH 12.4 (bottom), showing either discrete rod-like structures or vesicle-like particles and fibers (instead of vesicles or no aggregates); samples were analyzed ~10 months after their preparation.

Experimental procedure. 3 µL of sample solution was applied on plasma-treated (Gatan Solarus Model 950 Advanced Plasma System, p = 70 mTorr, H_2 flow 6.4 sccm, O_2 flow 27.5 sccm, forward RF target 50 W, time 30 s) carbon copper grids (Quantifoil R 3.5/1) in the environmental chamber of FEI Vitrobot having relative air humidity of 100 % and temperature of 22 °C. The excess solution was removed by blotting with filter paper for 1.5–2 seconds followed by 0–30 seconds draining and plunging of the samples into 1:1 mixture of liquid ethane and liquid propane, which was cooled below -170 °C. Vitrified samples were cryo-transferred into Jeol JEM-3200FSC cryo-transmission electron microscope operating at -194 °C. The temperature of the samples was -187 °C during the imaging. The microscope was operating in the bright field mode, using 300 kV acceleration voltage and the in-column energy filter set to 0–20 eV energy-loss range (zero-loss imaging). Micrographs were recorded with Gatan Ultrascan 4000 CCD camera.

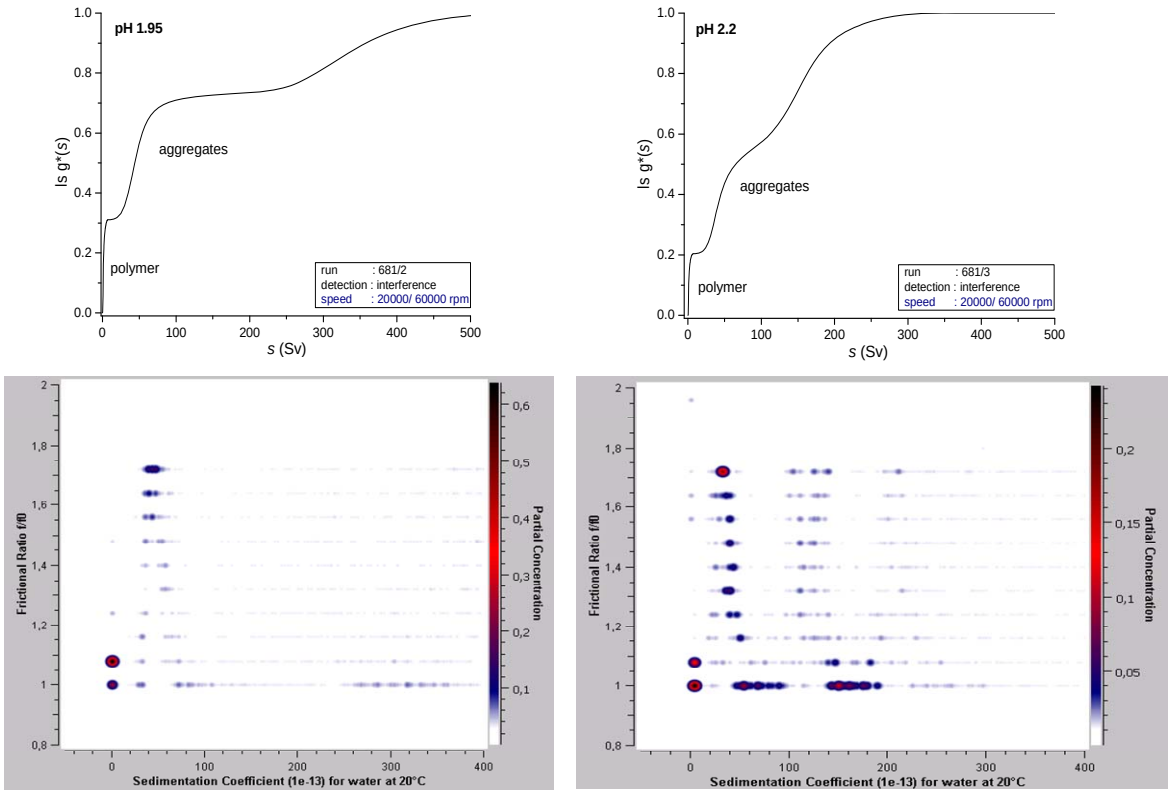

Figure S15. AUC sedimentation coefficient distributions (top) and pseudo 3D plots (UltraScan 2DSA-MC) of frictional ratio (f/f_o) *vs.* sedimentation coefficient (bottom) of aged ~0.1 wt% solutions of PEO_{42}-*b*-$PLLys_{61}$-*b*-$PLGlu_{62}$ in 0.5 M NaCl at pH 2.0 and pH 2.2; samples were analyzed ~3 months after their preparation.

Lamm equation fitting with 2DSA-MC analysis. Sedimentation and diffusion terms are used to generate solutions for the direct modeling of the sedimentation boundary, using the two dimensional spectrum analysis (2DSA) implemented in the software package UltraScan III. The frictional ratio (f/f_0), which gives a hint to the morphology of the sedimenting species, is determined with a model-free grid search followed by a Monte Carlo (MC) approach. It can be plotted as a function of the sedimentation coefficient in a pseudo 3D graph where the concentration of each species builds the pseudo z-axis (E. Brookes, W. Cao, B. Demeler, *Eur. Biophys. J.* **2010**, *39*, 405). Values of $f/f_0 \sim 1$ indicate structures with globular (spherical) shape whereas $f/f_0 \sim > 1$ indicate non-globular structures (*e.g.*, rods) (K. E. van Holde, W. C. Johnson, P. S. Ho, Principles of PhysicalBiochemistry, 2nd edition, Intl. ed., Prentice-Hall, EnglewoodCliffs, NJ 2005; C. R. Cantor, P. R. Schimmel, Biophysical Chemistry, Freeman Part II, San Francisco, CA 1980.). Exact dimensions of aggregates could not be determined because of different specific volumes of polymer chains and aggregates.

Calculations were performed on the UltraScan LIMS cluster at the Bioinformatics Core Facility at the University of Texas Health Science Center at San Antonio and XSEDE resources supported by NSF XSEDE Grant #MCB070038 (to Borries Demeler), and the Gateway is made possible by the use of XSEDE resources and Extended Collaborative Support Service (ECSS) Program funded by the NSF through the award OCI-1053575.